INTL JOURNAL OF ELECTRONICS AND TELECOMMUNICATIONS, 2014, VOL. 60, NO. 2, PP. 143–149
Manuscript received March 10, 2014; revised June, 2014. DOI: 10.2478/eletel-2014-0017

An Efficient Algorithm for Steady State Analysis of Fibre Lasers Operating under Cascade Pumping Scheme

Sławomir Sujecki

***Abstract*—We derive an efficient algorithm for the steady state analysis of fibre lasers operating under cascade pumping scheme by combining the shooting method with the Newton-Raphson method. We compare the proposed algorithm with the two standard algorithms that have been used so far in the available literature: the relaxation method and the coupled solution method. The results obtained show that the proposed shooting method based algorithm achieves much faster convergence rate at the expense of a moderate increase in the calculation time. It is found that a further improvement in the computational efficiency can be achieved by using few iterations of the relaxation method to calculate the initial guess for the proposed shooting method based algorithm.**

***Keywords*—photonics, fibre lasers, optical fibre technology, mid infra-red light technology, numerical modeling**

I. Introduction

FIBRE lasers have many characteristics that make them distinct from other types of light sources, i.e. hih brightness, wide tune-ability, ease of beam delivery and robustness. This makes them desirable in many applications. Commercially available silica glass fibre lasers cover wavelengths within the visible and near infrared range up to 2 μm. The longer wavelengths cannot be achieved in a silica glass host due to the depopulation of the upper lasing level via multi-phonon non-radiative transitions. In order to reach out to mid-infrared (MIR) wavelength region an application of a glass host with lower maximum phonon energy is necessary. So far commercially available ZBLAN fibres doped with erbium have been used successfully to realise lasers with operating wavelengths up to 3.9 μm [2]. Host glasses that would allow for the achievement of longer wavelengths are developed in the research laboratories. Currently one of the most promising glasses that is suitable for the realisation of long wavelength lasers is the chalcogenide glass. Chalcogenide glass fibres have been demonstrated to have very low loss within the MIR wavelength region [3] and to allow for a lanthanide doping of the fibre core [4] without inducing glass crystallisation.

Unlike the fibre lasers that operate within the visible and near-infrared range the MIR fibre lasers rely typically on the cascade pumping scheme (CPS). CPS allows the heat generation to be significantly reduced since all transitions between the relevant energy levels are radiative. Further, an improvement of laser efficiency can be achieved due to the idler wave contribution to the population inversion for the signal wave [5]. Fig.1 shows an example schematic diagram of the cascade pumping scheme. The pump increases the population of the level 3 at the expense of the population of the level 1. The signal interacts with the energy levels 2 and 3. The idler depletes the population of the level 2 and thus enhances the inversion of population for the signal wave. An example of a lanthanide element that operates within the pumping scheme illustrated in Fig.1 is a trivalent dysprosium ion. For other lanthanide elements it is possible that the idler facilitates the depletion of the level 3 while the signal interacts with the levels 2 and 1, e.g. Pr^{3+} [6].

The fibre lasers and amplifiers operating under the standard three level pumping schemes have been studied numerically for over twenty years now. Currently, the relaxation algorithm is best established as a tool for the numerical analysis and design of fibre lasers. This algorithm was subsequently adopted for the numerical analysis of the fibre lasers that operate under the cascade pumping scheme [5]. More recently the coupled solution method was adopted from the field of the numerical modelling of high power lasers [7]. Both techniques however, although fairly robust, have a low convergence rate. We therefore derive a shooting method based algorithm that is combined with the Newton-Raphson method. In the paper we compare the proposed shooting method based algorithm with both standard algorithms that have been used previously in the literature. The comparison is performed for a Dy^{3+} doped chalcogenide glass fibre laser that operates under the cascade pumping scheme, which was studied extensively in the literature [5, 7].

The paper is divided in four sections. After the introduction in the second section we provide the equations that describe the light interaction with the dysprosium ions within the chalcogenide glass fibre. In the third section we give the details of all three algorithms that are used in this study. In the fourth section we perform the comparison of the algorithms' performance. The last section provides a short summary of the main findings.

This work was supported European Commission through the Framework Seven (FP7) Project: MINERVA (317803; www.minerva-project.eu): MId-to NEaR infrared spectroscopy for improVed medical diagnostics.

S. Sujecki is with George Green Institute for Electromagnetics Research, Faculty of Engineering, University of Nottingham, Nottingham NG7 2RD, UK (e-mail: slawomir.sujecki@nottingham.ac.uk).

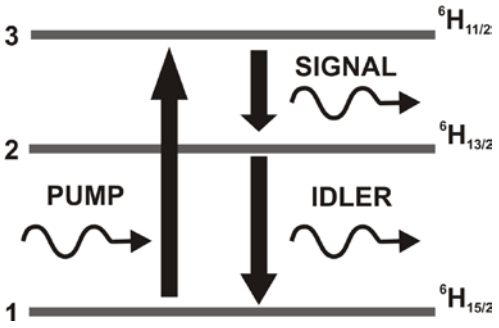

Fig. 1. Schematic diagram of Dy^{3+} energy level structure.

II. Laser Model

We consider three lowest levels for the trivalent dysprosium ion. The three-level model of the Dy^{3+} ion level populations is shown in Fig.1. Following [5], in order to calculate the populations of the energy levels, solution of the three associated coupled nonlinear differential equations is necessary. In steady state, these equations have the following form:

$$\begin{bmatrix} a_{11} & a_{12} & a_{13} \\ a_{21} & a_{22} & a_{23} \\ 1 & 1 & 1 \end{bmatrix} * \begin{bmatrix} N_1 \\ N_2 \\ N_3 \end{bmatrix} = \begin{bmatrix} 0 \\ 0 \\ N \end{bmatrix} \quad (1)$$

In (1) the coefficients a_{xx} are as follows: $a_{11} = \sigma_{pa}*\phi_p$; $a_{12} = \sigma_{\lambda 1a}*\phi(\lambda_1)$; $a_{13} = -\sigma_{pe}*\phi_p-\sigma_{\lambda 1e}*\phi(\lambda_1)-1/\tau_3$; $a_{21} = \sigma_{\lambda 2a}*\phi(\lambda_2)$; $a_{22} = -\sigma_{\lambda 2e}*\phi(\lambda_2)- \sigma_{\lambda 1a}*\phi(\lambda_1)-1/\tau_2$; $a_{23} = \sigma_{\lambda 1e}*\phi(\lambda_1) +\beta_{23}/\tau_3$ where τ_3 and τ_2 are the lifetimes of level 3 and 2, respectively, β_{32} is the branching ratio for the 3 -> 2 transition and $\sigma_{xya/e}$ is the absorption/emission cross-section for the xy transition. ϕ_p, $\phi(\lambda_1)$ and $\phi(\lambda_2)$ are the values of the optical intensity for the pump, signal and idler, respectively, at wavelengths λ_1 and λ_2, respectively. The optical intensities are related to optical powers by the following expressions: $\phi_p = P_p\ \Gamma_p\ \lambda_p/(A\ h\ c)$, $\phi(\lambda_1) = P(\lambda_1)\ \Gamma_{\lambda 1}\ \lambda_1/(A\ h\ c)$ and $\phi(\lambda_2) = P(\lambda_2)\ \Gamma_{\lambda 1}\ \lambda_1/(A\ h\ c)$, where A is the doping cross-section, h is Planck's constant, c is the speed of light in free space and Γ_x is the confinement factor [8].

In a fibre laser, the level populations are modified due to the strong photon densities associated with the optical waves trapped within the laser cavity. The spatial evolution of the powers for the pump, signal and idler powers are given through solution of the following ordinary differential equations:

$$\frac{dP_p^{\pm}}{dz} = \mp\Gamma_p\left[\sigma_{pa}N_1 - \sigma_{pe}N_3\right]P_p^{\pm} \mp \alpha\ P_p^{\pm} \quad (2a)$$

$$\frac{dP(\lambda_1)^{\pm}}{dz} = \mp\Gamma_{\lambda 1}\left[\sigma_{32a}N_2 - \sigma_{32e}N_3\right]P(\lambda_1)^{\pm} \mp \alpha\ P(\lambda_1)^{\pm} \quad (2b)$$

$$\frac{dP(\lambda_2)^{\pm}}{dz} = \mp\Gamma_{\lambda 1}\left[\sigma_{21a}N_1 - \sigma_{21e}N_2\right]P(\lambda_2)^{\pm} \mp \alpha\ P(\lambda_2)^{\pm} \quad (2c)$$

where '+' and '-' refer to forward and backward travelling waves, $P_p = P_p^+ + P_p^-$; $P(\lambda_1) = P(\lambda_1)^+ + P(\lambda_1)^-$ and $P(\lambda_2) = P(\lambda_2)^+ + P(\lambda_2)^-$.

The equations (2) are complemented by the following boundary conditions:

$$P_p^+(z=0) = r_p(z=0)P_p^-(z=0) \quad (3a)$$

$$P_p^-(z=L) = r_p(z=L)P_p^+(z=L) \quad (3b)$$

$$P^+(\lambda=\lambda_1, z=0) = r_{\lambda 1}(z=0)P^-(\lambda=\lambda_1, z=0) \quad (3c)$$

$$P^-(\lambda=\lambda_1, z=L) = r_{\lambda 1}(z=L)P^+(\lambda=\lambda_1, z=L) \quad (3d)$$

$$P^+(\lambda=\lambda_2, z=0) = r_{\lambda 2}(z=0)P^-(\lambda=\lambda_2, z=0) \quad (3e)$$

$$P^-(\lambda=\lambda_2, z=L) = r_{\lambda 2}(z=L)P^+(\lambda=\lambda_2, z=L) \quad (3f)$$

In order to calculate the output power of the fibre laser for a given value of the pump power, the equations describing the optical power evolution for the pump, signal and the idler (2) combined with the equations for the rare earth ionic level populations (1) have to be solved self-consistently. In the next section we present three algorithms that were implemented for this purpose.

III. Algorithms

In order to facilitate the discussion of the properties of the algorithms used to solve equations 1-3 we formally introduce a longitudinal discretisation along the fibre (Fig.2). Such discretisation is in fact automatically introduced when applying a numerical integration scheme to equations 2. We consider three algorithms: a relaxation method, a coupled solution method and a shooting method based algorithm.

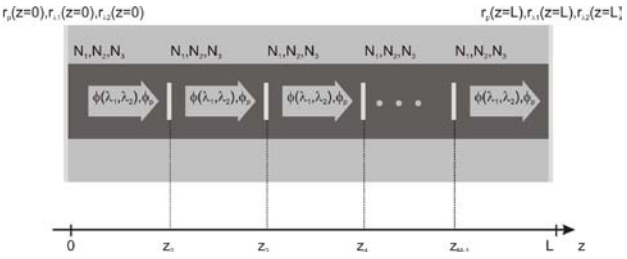

Fig. 2. Schematic diagram showing the longitudinal discretisation of the computational domain.

Algorithm 1 is effectively an adaptation of an algorithm that is very well-known in the field of high power laser modelling, i.e. the coupled solution method (CSM) [9]. CSM iterations start from initial values of pump, signal and idler powers for the forward propagating waves (FPWs) at z = 0. The initial values of power for the backward propagating waves (BPWs) are typically set to zero at all z positions (Fig.2). The equations (2) are first solved for the FPWs to calculate the values of power at z = L. In the second step equations (3) are used to calculate the powers of BPW at z = L. These power values are used as the initial values for equations (2), which are then integrated for BPWs to obtain the power values at z

=0. Finally, equations (3) yield FPW powers at z = 0. This process is continued until the values of FPW powers at z = 0 stop changing in the subsequent CSM iterations. Since, the application of standard numerical library routines for the integration of the ordinary differential equations (2) in the case of CSM is not straightforward we applied a local approximation, which assumes that the coefficients on the right hand side of (2) are locally constant and hence locally an exponential function approximation holds [10]. Thus essentially we approximate locally the set of differential equations (2) with a simple linear autonomous system of ordinary differential equations [11].

Algorithm 1: Dy^{3+} doped fibre laser model using coupled solution method

1. Start
2. Provide the initial values for forward propagating waves (FPWs): $P^+(\lambda=\lambda_1), P^+(\lambda=\lambda_2), P_p^+$ at z = 0
3. Set to 0 the power values of backward propagating waves (BPWs): $P^-(\lambda=\lambda_1), P^-(\lambda=\lambda_2), P_p^-$ for all z
4. Integrate equations (2) for FPWs and obtain $P^+(\lambda=\lambda_1), P^+(\lambda=\lambda_2), P_p^+$ at z = L (use latest available values of $P^-(\lambda=\lambda_1), P^-(\lambda=\lambda_2), P_p^-$)
5. Apply equations (3b),(3d) and (3f) to calculate $P^-(\lambda=\lambda_1), P^-(\lambda=\lambda_2), P_p^-$ at z=L
6. Integrate equations (2) for BPWs and obtain $P^-(\lambda=\lambda_1), P^-(\lambda=\lambda_2), P_p^-$ at z = 0 (use latest available values of $P^+(\lambda=\lambda_1), P^+(\lambda=\lambda_2), P_p^+$)
7. Apply equations (3a),(3c) and (3e) to calculate $P^+(\lambda=\lambda_1), P^+(\lambda=\lambda_2), P_p^+$ at z=0
8. Compare the calculated values of $P^+(\lambda=\lambda_1), P^+(\lambda=\lambda_2), P_p^+$ at z =0 with the previous ones. If the stop condition not fulfilled go to 4
9. Stop

The main disadvantage of the algorithm 1 is the necessity of storing the power values for FPWs and BPWs at all discrete z positions. Further, it is not straightforward to use standard numerical integration routines with CSM. However, applying the relaxation method (RM) is a simple remedy for these both shortcomings. For this purpose it is necessary to solve (2) simultaneously for both FPWs and BPWs when calculating the values of FPW powers at z = L using the FPW powers at z = 0 as initial values. Algorithm 2 summarises the main steps required for the implementation of the relaxation method.

The convergence rate of algorithms 1 and 2 may in some cases be very slow. Therefore we suggest a third algorithm that combines the shooting method (SM) with the Newton-Raphson method (NRM). For this purpose we first consider the following equations:

$$\begin{cases} P_p^+(L) - r_p P_p^+(L) = 0 \\ P_{s1}^+(L) - r_{\lambda 1} P_{s1}^+(L) = 0 \\ P_{s2}^+(L) - r_{\lambda 2} P_{s2}^+(L) = 0 \end{cases} \tag{4}$$

and introduce the following vector functions

$$\overline{P}^+(z) = \begin{bmatrix} P_p^+(z) \\ P_{s1}^+(z) \\ P_{s2}^+(z) \end{bmatrix}; \quad \overline{P}^-(z) = \begin{bmatrix} P_p^-(z) \\ P_{s1}^-(z) \\ P_{s2}^-(z) \end{bmatrix} \tag{5}$$

Equations (4) can be easily derived from the boundary condition (3). Observing that due to (2) equations (4) can be rewritten in the following way:

$$\begin{cases} P_p^+\left(\overline{P}^-(0), \overline{P}^+(0)\right) - r_p P_p^+\left(\overline{P}^-(0), \overline{P}^+(0)\right) = 0 \\ P_{s1}^+\left(\overline{P}^-(0), \overline{P}^+(0)\right) - r_{\lambda 1} P_{s1}^+\left(\overline{P}^-(0), \overline{P}^+(0)\right) = 0 \\ P_{s2}^+\left(\overline{P}^-(0), \overline{P}^+(0)\right) - r_{\lambda 2} P_{s2}^+\left(\overline{P}^-(0), \overline{P}^+(0)\right) = 0 \end{cases} \tag{6}$$

The set of 3 nonlinear equations (6) has 6 unknowns. However, using (3) one can easily reduce the number of unknowns to 3 by calculating the elements of the vector $\overline{P}^-$ from the elements of the vector $\overline{P}^+$ at z =0. Thus we obtain 3 equations with 3 unknowns:

$$\begin{cases} E_1\left(\overline{P}^+(0)\right) = P_p^+\left(\overline{P}^+(0)\right) - r_p P_p^+\left(\overline{P}^+(0)\right) = 0 \\ E_2\left(\overline{P}^+(0)\right) = P_{s1}^+\left(\overline{P}^+(0)\right) - r_{\lambda 1} P_{s1}^+\left(\overline{P}^+(0)\right) = 0 \\ E_3\left(\overline{P}^+(0)\right) = P_{s2}^+\left(\overline{P}^+(0)\right) - r_{\lambda 2} P_{s2}^+\left(\overline{P}^+(0)\right) = 0 \end{cases} \tag{7}$$

Algorithm 2: Dy^{3+} doped fibre laser model using relaxation method

1. Start
2. Provide the initial values for FPW and BPW powers at z = 0
3. Integrate equations (2) for FPWs and BPWs and obtain $P^+(\lambda=\lambda_1), P^+(\lambda=\lambda_2), P_p^+$ and $P^-(\lambda=\lambda_1), P^-(\lambda=\lambda_2), P_p^-$ at z = L
4. Apply equations (3b),(3d) and (3f) to calculate $P^-(\lambda=\lambda_1), P^-(\lambda=\lambda_2), P_p^-$ at z=L from $P^+(\lambda=\lambda_1), P^+(\lambda=\lambda_2), P_p^+$
5. Integrate equations (2) for FPWs and BPWs and obtain $P^+(\lambda=\lambda_1), P^+(\lambda=\lambda_2), P_p^+$ and $P^-(\lambda=\lambda_1), P^-(\lambda=\lambda_2), P_p^-$ at z = 0
6. Apply equations (3a),(3c) and (3e) to calculate $P^+(\lambda=\lambda_1), P^+(\lambda=\lambda_2), P_p^+$ at z=0 from $P^-(\lambda=\lambda_1), P^-(\lambda=\lambda_2), P_p^-$
7. Compare the calculated values of $P^+(\lambda=\lambda_1), P^+(\lambda=\lambda_2), P_p^+$ at z =0 with the previous ones. If the stop condition not fulfilled go to 3
8. Stop

The solution of equation (7) can be obtained using the Newton-Raphson method (NRM). Using vector notation (7) can be expressed in the following compact way:

$$\overline{E}\left(\overline{P}^+(0)\right)=\begin{bmatrix} E_1\left(\overline{P}^+(0)\right) \\ E_2\left(\overline{P}^+(0)\right) \\ E_3\left(\overline{P}^+(0)\right) \end{bmatrix}$$

Since the analytical expressions for equations E_1, E_2 and E_3 in (7) are only given implicitly via the solution of the initial value problem (3) for the FPWs, the analytical calculation of the Jacobian is very complicated. We therefore use the finite difference (FD) approach from [1] with FD step size equal to 10^{-4}. Once the Jacobian J is known the updates of the FPW powers at z = 0 can be obtained from:

$$[J]\Delta P_{iter}^+ = -\overline{E}\left(\overline{P}_{iter}^+(0)\right) \quad (8a)$$

$$\overline{P}_{iter+1}^+(0) = \overline{P}_{iter}^+(0) + \Delta\overline{P}_{iter}^+ \quad (8b)$$

In (8) we have placed J in square brackets to indicate that the Jacobian J is a 3x3 matrix. The index 'iter' in (8) keeps the track of subsequent NRM iterations. Lastly we note that the BPW powers at z = 0 can be obtained from (3). Algorithm 3 below gives the implementation details of the SM with NRM.

Algorithm 3: Dy^{3+} doped fibre laser model using shooting method

1. Start
2. Provide the initial values for FPW and BPW powers at z = 0
3. Use equations (3a),(3c) and (3e) to calculate consistently initial values for backward propagating waves (BPWs) $P^-(\lambda=\lambda_1), P^-(\lambda=\lambda_2), P_p^-$ at z=0
4. Integrate equations (2) for FPWs and BPWs and obtain $\overline{E}\left(\overline{P}_{iter}^+(0)\right)$ for (8a)
5. Apply FD method [1] to obtain the Jacobian elements for (8a)
6. Solve the set of 3 linear algebraic equations (8a) and obtain new values of FPW powers at z = 0 from (8b)
7. Apply equations (3a),(3c) and (3e) to calculate BPW powers at z =0
8. Compare the calculated values of $P^+(\lambda=\lambda_1), P^+(\lambda=\lambda_2), P_p^+$ at z =0 with the previous ones. If the stop condition not fulfilled go to 4
9. Stop

Lastly, we discuss the condition for termination of the iterations. For this purpose we calculate the residual as the square of the l_2 norm of the vector obtained from the difference between the values of $\overline{P}^+$ at z =0 from the last and previous iterations, i.e. the norm of the vector $\Delta\overline{P}_{iter}^+$ from equation (8b) [12]. The residual can be used to terminate the iterations once it reaches a predefined level.

IV. Results

As an example of a fibre laser with the cascade pumping scheme we consider a Dy^{3+} chalcogenide glass fibre laser. The Dy^{3+} chalcogenide glass fibre laser structure was selected here since it is very often discussed in the literature [5-7]. The cavity structure for the fibre laser is shown in Fig.3. The idler and signal waves are reflected from the fibre ends due to Fresnel reflection. This simple fibre laser structure originally proposed and studied in [7].

Fig. 3. Schematic diagram of the fibre laser cavity used for simulations.

It is convenient for the forthcoming analysis and discussion to identify different regions of fibre laser operation under the cascade pumping scheme. Fig.4 shows a typical dependence of the signal and idler output power on the pump power. In this plot two regions of the laser operation can be identified. Region I corresponds to the laser operation below the idler threshold. The laser operation within region I is characterised by a relatively slow growth of the signal output power. In the region II both idler and signal are above threshold. In region II the laser slope efficiency is enhanced due to the idler contribution to the population inversion of the signal wave. We apply all three algorithms to both the region I and II in Fig.4.

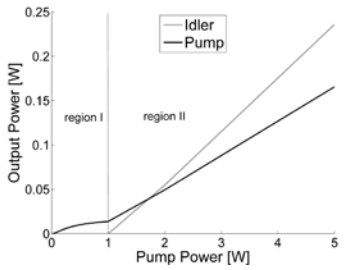

Fig. 4. Typical dependence of the idler and signal power on the pump power for a fibre laser operating under cascade pumping scheme.

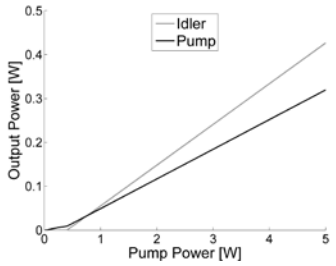

Fig. 5. Numerically calculated dependence of the idler and signal power on the pump power for a fibre laser parameters listed in Table 1.

The simulation parameters are listed in Table 1. Fig. 5 shows the calculated dependence of the idler and signal power on the pump power for the fibre laser with parameters listed in Table 1. For the discussion that follows we select 2 values of the pump power in the region I, i.e. 0.2 W and 0.4 W and 2 values in the region II: 1 W and 5 W. For the selected values of the pump power, Table 2 gives the values of signal and idler power that are believed to be calculated accurately on at least 12 digital places. These reference results were obtained using algorithm 3 with the standard Matlab ode45 Dormand and Prince version of the Runge-Kutta (5)4 algorithm [13]. The relative and absolute tolerances were set to 10^{-13}.

TABLE I
SIMULATION PARAMETERS FOR A Dy^{3+} CHALCOGENIDE GLASS FIBRE LASER FROM FIG.3

Quantity	Value	Unit
Dy^{3+}-ion concentration	$7x10^{19}$	cm^{-3}
Core radius	5.5	μm
Numerical aperture	0.2	
Cladding radius	30	μm
Fibre length L	2.1	m
Fibre loss at all wavelengths	1	dB/m
Lifetime of level 3	2	ms
Lifetime of level 2	5.2	ms
Branching ratio for 3-2 transitions	0.15	
reflectivity for idler, signal and pump at z = 0	0.2	
reflectivity for idler, signal and pump at z = L	0.2	
Confinement factor for signal (λ_1)	0.8	
Confinement factor for idler (λ_2)	0.9	
Confinement factor for pump	0.034	
Pump wavelength	1.71	μm
Signal wavelength (λ_1)	4.6	μm
Idler wavelength (λ_2)	3.35	μm
Pump emission cross section	$0.318x10^{-20}$	cm^2
Pump absorption cross section	$0.501x10^{-20}$	cm^2
Idler emission cross section	$0.912x10^{-20}$	cm^2
Idler absorption cross section	$0.485x10^{-20}$	cm^2
Signal emission cross section	$0.097x10^{-20}$	cm^2
Signal absorption cross section	$0.016x10^{-20}$	cm^2

TABLE II
REFERENCE VALUES OF SIGNAL AT IDLER POWER CALCULATED BY SM-NRM FOR THE FIBRE LASER PARAMETERS FROM TABLE I

Pump power	Signal power	Idler power
0.2 W	$4.732684968926743x10^{-3}$ W	0 W
0.4 W	$8.744905834624988x10^{-3}$ W	0 W
1 W	$4.893233642458401x10^{-2}$ W	$5.505718865901951x10^{-2}$ W
5 W	$3.183467070903177x10^{-1}$ W	$4.249980254830068x10^{-1}$ W

Figs.6-9 show the dependence of the residual, CPU time, and absolute error on the iteration number for the three algorithms studied: algorithm 1 – Coupled Solution Method (CSM), algorithm 2 – Relaxation Method (RM), algorithm 3 – Shooting Method combined with Newton-Raphson Method (SM-NRM). We performed calculations at the selected four pump power values from Table 2. The absolute error was calculated as a absolute value of the difference between the calculated result and the reference result taken from the table 2. Algorithms 2 and 3 use the standard Matlab ode45 routine to integrate ordinary differential equations (2) while algorithm 1 uses, as mentioned in the previous section, the

local approximation with the Exponential Function Solution (EFS). The relative and absolute tolerance for ode45 was kept equal to 10^{-13} while EFS was used with 1000 equidistant longitudinal steps. The initial values of the pump, idler and signal powers for all 3 algorithms were set to:

$$\begin{aligned} &P_p^+(z=0) = w\ P_p \\ &P^+(\lambda=\lambda_1, z=0) = 0.2\ \ P_p^+(z=0) \\ &P^+(\lambda=\lambda_2, z=0) = 0.2\ \ P_p^+(z=0) \\ &P_p^-(z=0) = 0 \\ &P^-(\lambda=\lambda_1, z=0) = 0 \\ &P^-(\lambda=\lambda_2, z=0) = 0 \end{aligned} \tag{9}$$

where Pp is the pump power (Fig.2) and w =0.8.

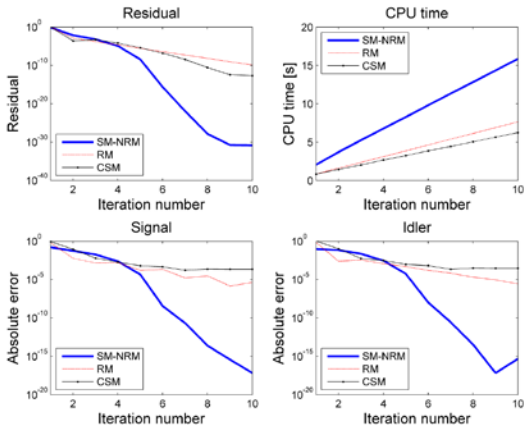

Fig. 6. Numerically calculated dependence of the residual, CPU time and absolute error for the three algorithms studied: algorithm 1 – Coupled Solution Method (CSM), algorithm 2 – Relaxation Method (RM), algorithm 3 – Shooting Method combined with Newton-Raphson Method (SM-NRM). The calculation parameters are listed in Table 1, while the pump power equals 5 W.

The results from Figs.6-9 show that the calculation time for SM-NRM is approximately twice the time needed for CSM and RM. The convergence rate of the SM-NRM is initially comparable with the other algorithms. However, after few initial iteration steps the convergence of SM-NRM improves significantly and is far superior when compared with CSM and RM. It can be also observed that the slowest convergence takes place near the idler threshold (at 0.4 W). In this case it took nearly 8 SM-NRM iterations before the onset of the fast convergence. The convergence rate of RM and CSM is similar. However, in CSM results one can observe a flattening of the error dependence for larger values of the iteration number. This behaviour is caused by the limited accuracy of the EFS approximation. A simple remedy for this effect is an increase of the longitudinal steps' number. The penalty for this however, is a significant increase of the calculation time, which would render this algorithm relatively inefficient. More effective solution of the problem would require an application of a more efficient numerical integration scheme, c.f. [11, 14].

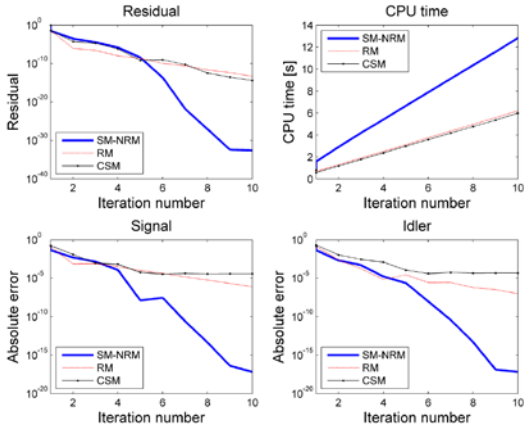

Fig. 7. Numerically calculated dependence of the residual, CPU time and absolute error for the three algorithms studied: algorithm 1 – Coupled Solution Method (CSM), algorithm 2 – Relaxation Method (RM), algorithm 3 – Shooting Method combined with Newton-Raphson Method (SM-NRM). The calculation parameters are listed in Table 1, while the pump power equals 1 W.

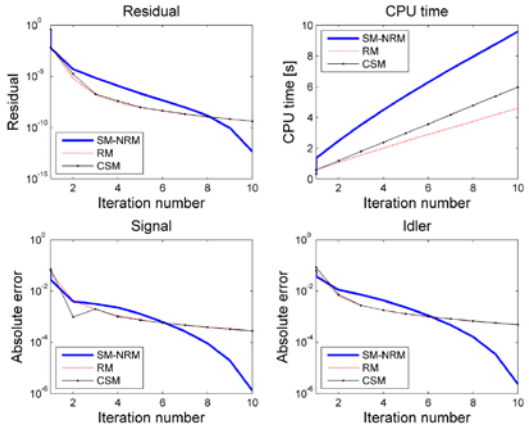

Fig. 8. Numerically calculated dependence of the residual, CPU time and absolute error for the three algorithms studied: algorithm 1 – Coupled Solution Method (CSM), algorithm 2 – Relaxation Method (RM), algorithm 3 – Shooting Method combined with Newton-Raphson Method (SM-NRM). The calculation parameters are listed in Table 1, while the pump power equals 0.4 W.

Further improvement of the algorithm performance can be obtained by applying the RM for the calculation of the initial guess of the SM-NRM. This idea can be deduced from the results shown in Figs.6-9. Since during the initial iteration steps the convergence rate of RM and SM-NRM is similar while the calculation time of RM is less an increase in the overall efficiency of the algorithm can be expected by using RM instead of SM-NRM during the initial iteration steps and switching to SM-NRM when the region of the fast convergence is reached.

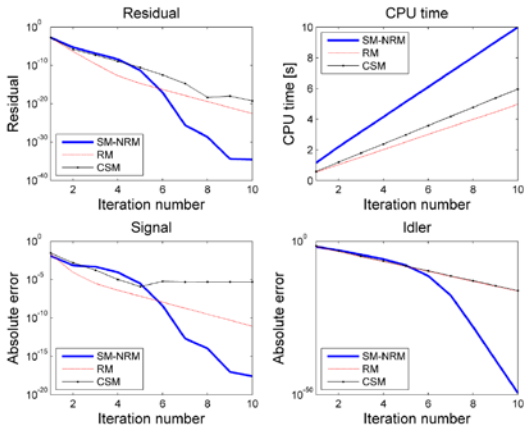

Fig. 9. Numerically calculated dependence of the residual, CPU time and absolute error for the three algorithms studied: algorithm 1 – Coupled Solution Method (CSM), algorithm 2 – Relaxation Method (RM), algorithm 3 – Shooting Method combined with Newton-Raphson Method (SM-NRM). The calculation parameters are listed in Table 1, while the pump power equals 0.2 W.

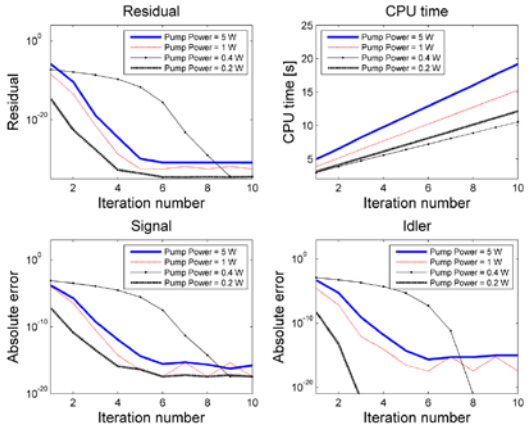

Fig. 10. Numerically calculated dependence of the residual, CPU time and absolute error for the algorithm 3, i.e. Shooting Method combined with Newton-Raphson Method (SM-NRM) whereby the initial guess was calculated by 4 iterations of algorithm 2 – Relaxation Method (RM). The calculation parameters are listed in Table 1.

In Fig.10 we have therefore studied a SM-NRM algorithm that uses 4 RM iterations to refine the initial guess. As expected, the time required to complete the first iteration increased when compared with Figs.6-9. This is because additional 4 RM iterations need to be completed. However, for the relatively slowly converging results, at the pump powers below the idler threshold, the onset of the fast convergence is taking place several iterations earlier than in the results shown in Figs.6-9. The overall CPU time needed for completing 10 iterations however, is only marginally larger. It was also observed the algorithm that combines SM-NRM with RM is less sensitive to the choice of the initial guess than the SM-NRM.

V. Conclusions

We developed an algorithm for the analysis of the fibre lasers operating under the cascade pumping scheme that is based on the combination of the shooting method with the Newton-Raphson method (SM-NRM). The developed algorithm converges faster than the standard methods reported so far in the available literature. It was also shown that the further improvement of the algorithm performance can be obtained by combining SM-NRM with the relaxation method (RM).

References

[1] W.H. Press, S.A. Teukolsky, W.T. Vetterling, and B.P. Flannery, “Numerical recipes in C^{++}: the art of scientific computing,” Cambridge: Cambridge University Press, 2002.

[2] J. Schneider, C. Carbonnier and U.B. Unrau, “Characterization of a Ho^{3+}-doped fluoride fiber laser with a 3.9-μm emission wavelength,” Applied Optics, vol 36, no. 33, pp. 8595-8600, Nov. 1997.

[3] G. E. Snopatin, M. F. Churbanov, A. A. Pushkin, V. V. Gerasimenko, E. M. Dianov, and V. G. Plotnichenko, “High purity arsenic-sulfide glasses and fibers with minimum attenuation of 12 dB/km,” Optoelectronics and Advanced Materials-Rapid Communications, vol.3, no. 7, pp. 669-671. Jul. 2009.

[4] L. Sojka, Z. Tang, D. Furniss, H. Sakr, A. Oladeji, E. Beres-Pawlik, H. Dantanarayana, E. Faber, A. B. Seddon, T. M. Benson, and S. Sujecki, “Broadband, mid-infrared emission from Pr^{3+} doped GeAsGaSe chalcogenide fiber, optically clad,” Optical Materials, vol. 36, no. 6, pp. 1076-1082, April 2014.

[5] R.S. Quimby, L. B. Shaw, J.S. Sanghera, and I.D. Aggarwal, “Modeling of cascade lasing in Dy : Chalcogenide glass fiber laser with efficient output at 4.5 μm,” IEEE Photonics Technology Letters, vol. 20, no. 1-4, pp. 123-125, Jan. 2008.

[6] L. Sojka, Z. Tang, H. Zhu, E. Beres-Pawlik, D. Furniss, A.B. Seddon, T.M. Benson, and S. Sujecki, “Study of mid-infrared laser action in chalcogenide rare earth doped glass with Dy^{3+}, Pr^{3+} and Tb^{3+},” Optical Materials Express, vol. 2, no. 11, pp. 1632-1640, Nov. 2012.

[7] S. Sujecki, L. Sójka, E. Bereś-Pawlik, Z. Tang, D. Furniss, A.B. Seddon, and T.M. Benson, “Modelling of a simple Dy^{3+} doped chalcogenide glass fibre laser for mid-infrared light generation,” Optical and Quantum Electronics, 2010. Vol. 42, no.2 , pp. 69-79, Jan. 2010.

[8] P.C. Becker, N.A. Olsson, and J.R. Simpson, “Erbium doped fiber amplifiers. Fundamentals and Technology,” 1999, London: Academic Press.

[9] S. Sujecki, L. Borruel, J.Wykes, P. Moreno, B. Sumpf, P. Sewell, H. Wenzel, T.M. Benson, G. Erbert, I. Esquivias, and E. C. Larkins, “Nonlinear properties of tapered laser cavities,” IEEE Journal of Selected Topics in Quantum Electronics, vol. 9, no. 3, pp. 823-834, May/June 2003.

[10] S. Sujecki, “Stability of steady-state high-power semiconductor laser models,” Journal of Optical Society of America B, vol. 24, no. 5, pp. 1053-1060, May 2007.

[11] C. Pozirikidis, “Numerical Computation in Science and Engineering,” Oxford: Oxford University Press, 1998.

[12] G.D. Smith, “Numerical Solution of Partial Differential Equations: Finite Difference Method,” Oxford: Oxford University Press, 1988.

[13] J.R. Dormand and P.J.Prince, “A family of embedded Runge-Kutta formulae,” J. Comp. Appl. Math, vol. 6, no. 1, p. 19-26, 1980.

[14] S. Rosloniec, “Fundamental Numerical Methods for Electrical Engineering,” Berlin: Springer, 2008.